The role of geosynthetic stiffness in soil reinforcement applications

Richard J. Bathurst[1*], *Fahimeh M.* Naftchali[2], and *Reza* Jamshidi Chenari[1]

[1]GeoEngineering Centre at Queens-RMC, Civil Engineering Department, Royal Military College of Canada, Kingston, Ontario, Canada
[2]GeoEngineering Centre at Queens-RMC, Civil Engineering Department, Queen's University, Kingston, Ontario, Canada

Abstract. Most often the focus on the mechanical contribution of reinforcement geosynthetics in soil reinforcement applications has been on the strength of the material. In fact, under operational conditions the performance of these systems is controlled by the stiffness of the geosynthetic, not its strength. An appreciation of the role of geosynthetic stiffness in soil reinforcement applications is complicated by the rate-dependency of many products which means that their load-strain properties are time-, strain- and temperature-dependent. This paper describes the quantification of these properties using a simple isochronous load-strain model with properties fitted from laboratory creep testing. The implementation of the model and its consequences on the quantitative performance of mechanically stabilized earth (MSE) wall loads and deformations, reinforced fills over voids, and a thin reinforced granular base over a soft clay foundation are demonstrated.

1 Introduction

Geosynthetic sheet reinforcement products are now well-established in geotechnical earthworks engineering to improve the strength and stiffness of the soil. Analytical models for the estimation of facing deformations and reinforcement loads in mechanically stabilized earth (MSE) walls under operational (in-service) conditions, reinforced fills over voids, and the problem of a reinforced granular base over soft undrained clay foundations are just four examples. Most often, the extensible reinforcement layers are assumed to behave as linear-elastic plastic materials in these formulations. However, geosynthetic reinforcement materials are rate-dependent materials to different degrees meaning that their tensile load-strain properties are load-, strain-, temperature-, and time-dependent. This paper reviews recent work by the writers that introduces a two-component hyperbolic model to quantify the isochronous tensile stiffness of a geosynthetic reinforcement product. The model is then used in existing analytical models to predict facing deformations and reinforcement loads in geosynthetic MSE walls under operational conditions, mobilized reinforcement stiffness in reinforced granular fills over voids, and in a numerical model of a footing seated on a reinforced granular base over a soft clay foundation. These examples highlight the sensitivity of analysis and design outcomes to the choice of stiffness model parameter values.

* Corresponding author: bathurst-r@rmc.ca

2 Geosynthetic stiffness

The earliest attempt to characterize the load-strain time behaviour of extensible geosynthetic sheet reinforcement products under constant tensile load can be traced to the seminal work of McGown et al. [1, 2]. They introduced the concept of isochronous load-strain curves. The construction of isochronous curves from constant-load creep tests is illustrated in Figure 1a and 1b. The construction of the corresponding isochronous secant stiffness curves is shown in Figure 1c.

2.1 Two-component isochronous stiffness model

Each curve in Figure 1b can be approximated by a hyperbolic equation of the following form [3]:

$$T(\varepsilon,t)=\frac{\varepsilon}{\frac{1}{J_o(t)}+\frac{1}{\chi(t)}\varepsilon} \qquad (1)$$

Here, t is isochronous time, $J_o(t)$ is the initial stiffness at zero strain, and $\chi(t)$ is a parameter that captures the curvature of the isochronous curve. As $1/\chi(t) \rightarrow 0$, isochronous curves become linear. In analytical modelling of reinforced soil structures the calculation of T is related to strain according to the secant isochronous stiffness $J(\varepsilon, t)$:

$$T(\varepsilon,t)=J(\varepsilon,t)\times\varepsilon \qquad (2)$$

From Equations 1 and 2, the secant stiffness as a function of strain for an isochronous curve is:

$$J(\varepsilon,t)=\frac{1}{\frac{1}{J_o(t)}+\frac{1}{\chi(t)}\varepsilon} \qquad (3)$$

Secant stiffness values are used in analytical models as demonstrated later in the paper. The tangent stiffness at the same strain on an isochronous curve is computed by differentiation to give:

$$J_t(\varepsilon,t)=\frac{1}{J_o(t)\left[\frac{1}{J_o(t)}+\frac{1}{\chi(t)}\varepsilon\right]^2} \qquad (4)$$

Tangent stiffness values are required for the step-wise implementation of non-linear constitutive models in numerical finite element and finite difference method codes.

Bathurst and Naftchali [3] collected more than 600 high-quality constant-load creep tests performed on 89 different geosynthetic reinforcement products. They classified the products into seven classification types; (1) high-density polyethylene (HDPE) punched and drawn geogrid, (2) polyester (PET) woven and knitted geogrid, (3) polypropylene (PP) punched and drawn geogrid, (4) PP woven geotextile, (5) PET woven geotextile, (6) PET nonwoven geotextile, and (7) PET strap. The tests were carried out in general conformity with ASTM D5262-97 and ASTM D6992-03 test standards [4, 5].

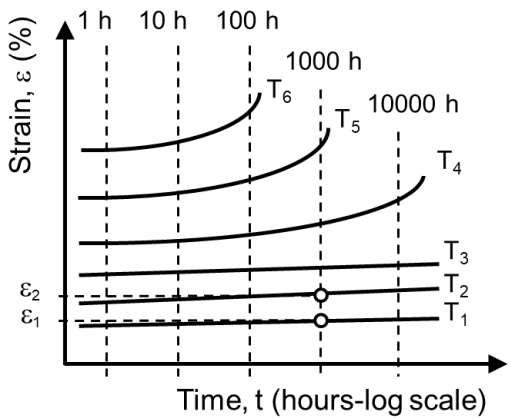

a)

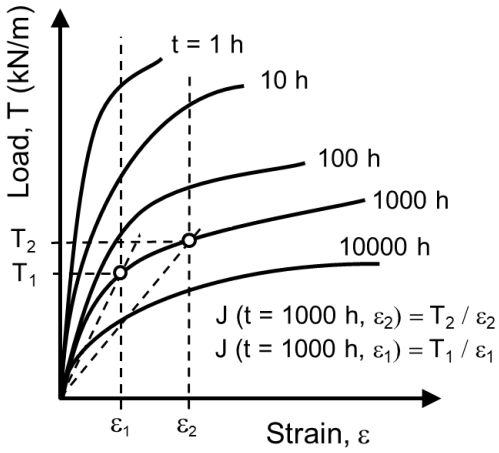

b)

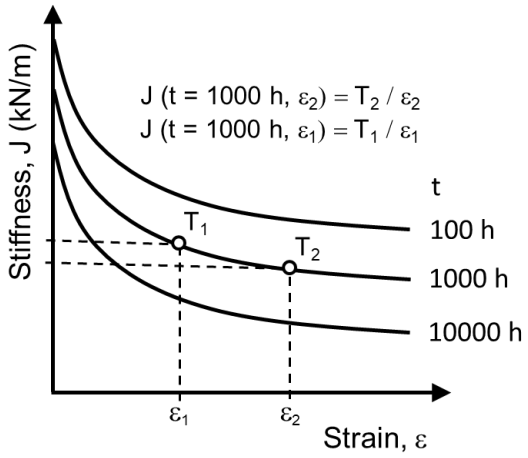

c)

Fig. 1. Interpretation of load-strain-time data from: a) constant-load creep tests; b) isochronous load-strain curves showing secant stiffness, and c) isochronous secant stiffness curves [3].

Figure 2a shows isochronous load-strain curves for a PP punched and drawn biaxial geogrid. The right vertical axis is the tensile load expressed as percentage of the reference index tensile strength deduced from a conventional constant rate-of-strain (CRS) test at 10% strain per minute (ASTM D4595-17 or ASTM D5262-97 methods of test [6, 7], or equivalent). As expected, the curves become shallower as the isochronous time increases. The corresponding isochronous secant stiffness curves are shown in Figure 2b.

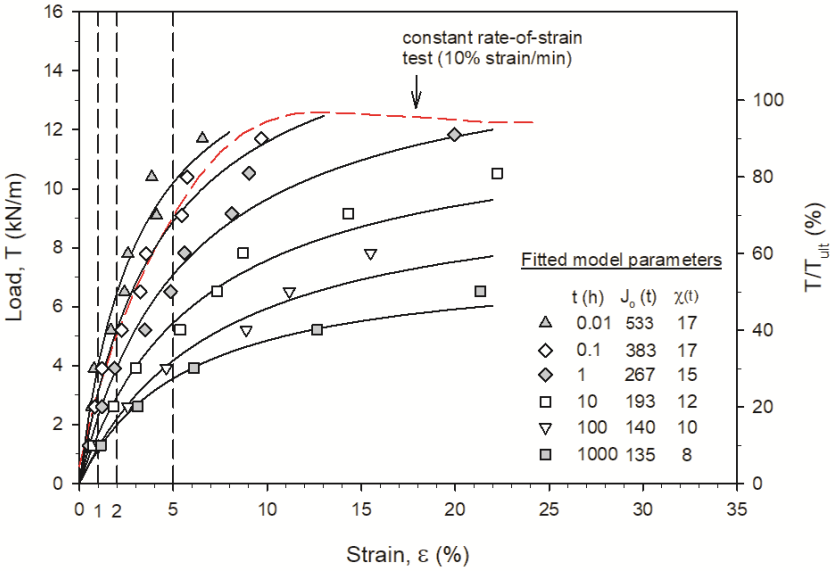

a)

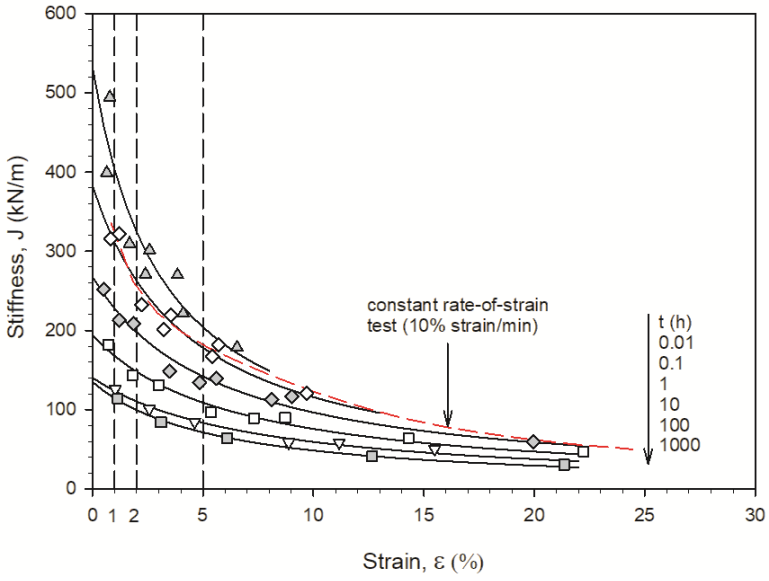

b)

Fig. 2. Biaxial PP geogrid: a) isochronous curves, b) secant stiffness curves. Note: Parameters $J_o(t)$ and $\chi(t)$ have units of kN/m [3].

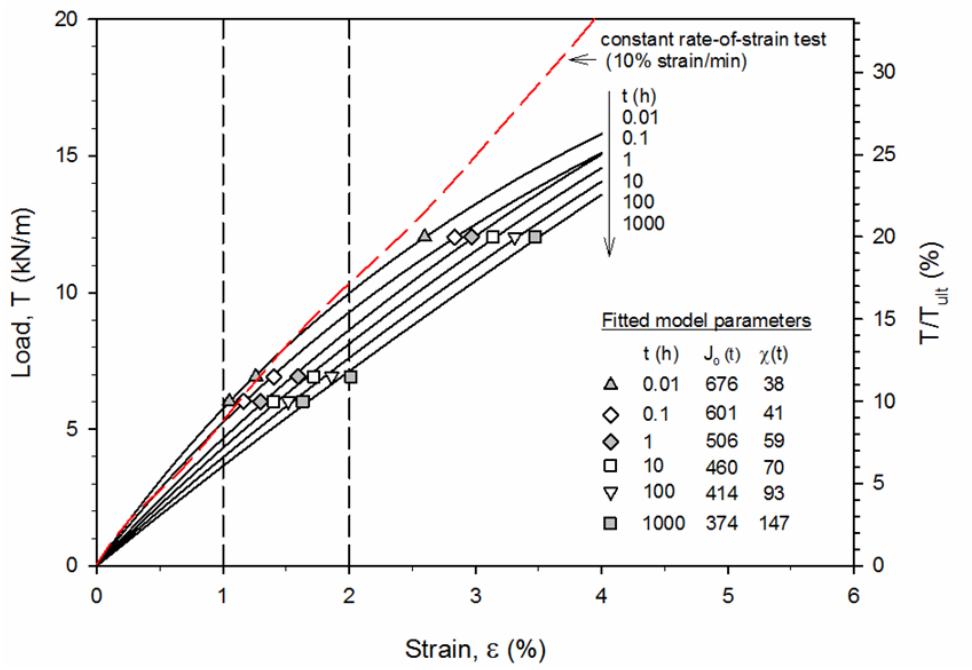

a)

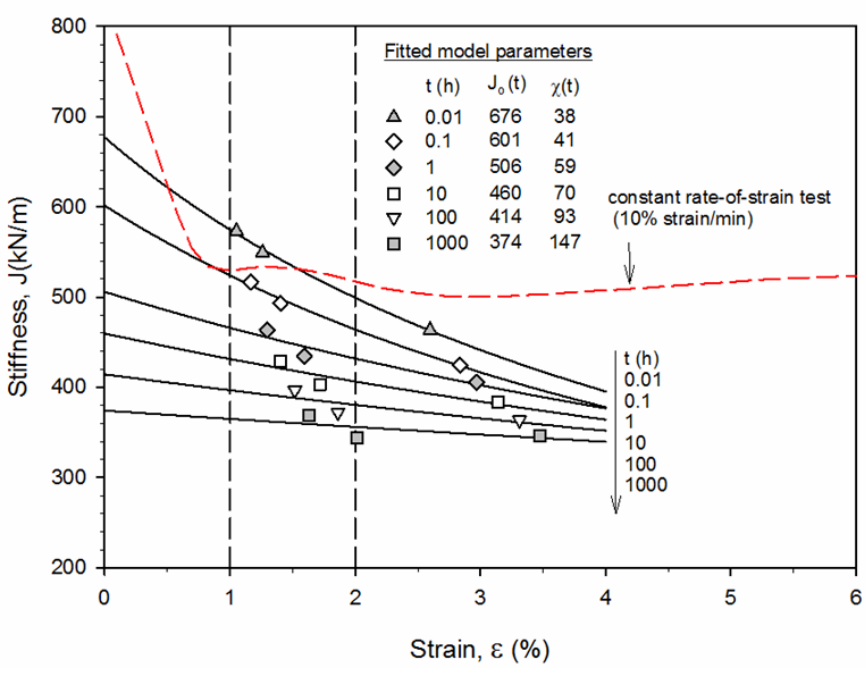

b)

Fig. 3. PET woven geogrid: a) isochronous curves, b) secant stiffness curves. Note: Parameters $J_o(t)$ and $\chi(t)$ have units of kN/m [3].

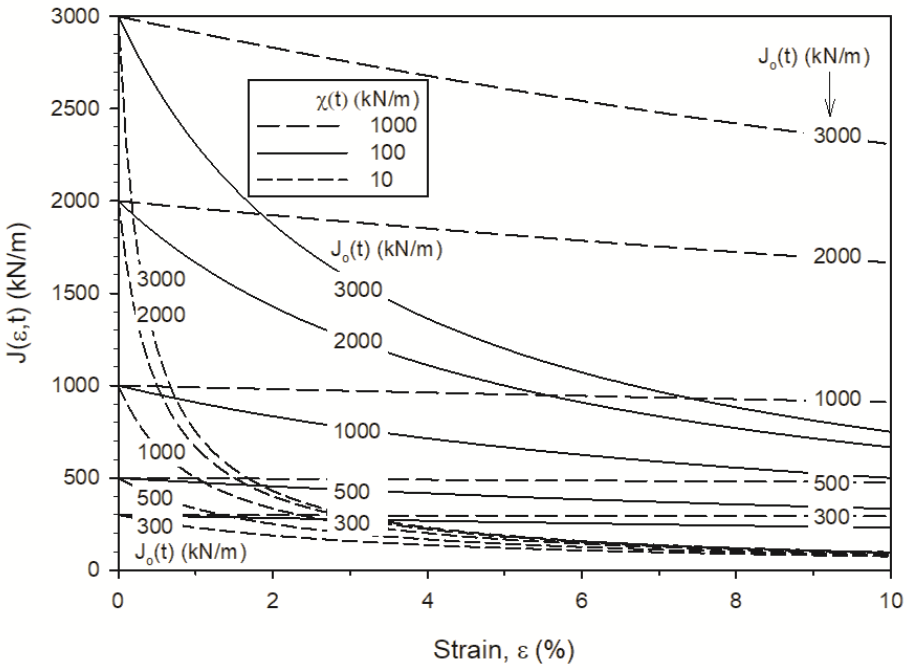

Fig.4. Influence of $J_o(t)$ and $\chi(t)$ on isochronous stiffness at the same isochronous time [8].

These curves show that as isochronous time and strain increase, the stiffness decreases. The isochronous stiffness curves can be seen to converge with increasing strain. An important observation from these plots is that load and stiffness at a given strain using the load-strain curve from the conventional CRS tensile test is greater than the isochronous load and stiffness at practical isochronous times (e.g., 1000 h). Thus, using rapid in-air CRS tests will result in an over-estimate of reinforcement stiffness for this product. The same observation to different degrees was made for the other geosynthetic products in the database compiled by Bathurst and Naftchali [3].

Similar analysis results are presented in Figure 3 for a PET woven geogrid. These data present with flatter curves.

The two-component hyperbolic model can be used to quantify a range of behaviour including PET strap materials which exhibit increasing stiffness during initial loading due to the macro-scale tightening of the aligned PET filament bundles [3].

The influence of magnitude of the stiffness term $J_o(t)$ and curvature parameter $\chi(t)$ is illustrated in Figure 4. Typical ranges for these parameters for sheet reinforcement products are summarized in Figure 5 [3, 8].

2.2 Approximations to isochronous secant stiffness using ultimate tensile strength

Creep-data of the type and quality collected by Bathurst and Naftchali [3] to calibrate hyperbolic stiffness model parameters may not always be available. They developed useful correlations between isochronous stiffness at different times and different strain levels of 1%, 2%, 3%, 4% and 5%, and the index ultimate tensile strength (T_{ult}) of the product using conventional 10% strain per minute CRS tests. Example results for 2% strain are presented in Figures 6a and 6b, using linear and power function approximations, respectively. The

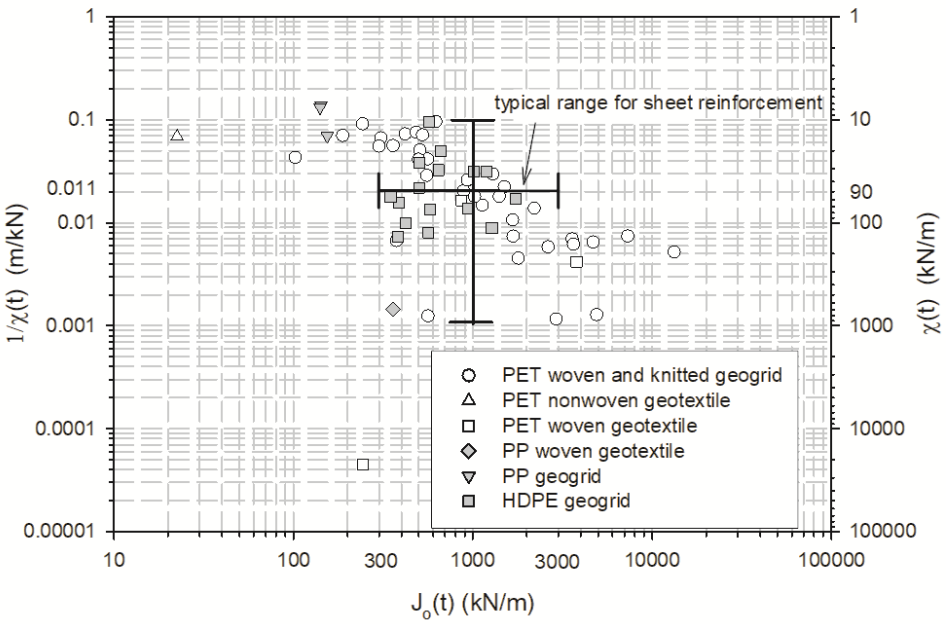

Fig. 5. Isochronous curvature [$1/\chi(t)$ or $\chi(t)$] versus initial tangent stiffness $J_o(t)$ for t = 1000 h. Data from [3, 8].

coefficients for the two function types vary depending on the material type as demonstrated in the figure legends. However, a useful first approximation for preliminary analysis purposes and isochronous time t = 1000 h and ε = 2%, is $J = 5 \times T_{ult}$ (Figure 6a).

3 Examples

In this section the influence on analysis and design outcomes for four different reinforced soil applications using different geosynthetic secant stiffness values described by parameters $J_o(t)$ and $\chi(t)$ is demonstrated.

In the wall examples to follow the wrapped-face wall geometry in Figure 7 is used [9].

3.1 Wall displacements

A first-order approximation of end-of-construction wall out-of-alignment with respect to the toe can be made using the method of Jewell and Milligan [10]. Consider the case of an unsurcharged vertical MSE wall (Figure 7) of height H_w = 6 m with a single reinforcement type with constant stiffness J, constant length $L = 0.7H_w$, and layers placed at uniform vertical spacing (S_v) with a wrapped-face configuration. The wall outward deformation Δh at layer depth z below the crest of the wall can be computed as:

$$\Delta_h = \frac{K_a S_v \gamma z (H_w - z)}{3(J \times S_r)} \left[\tan(45° - \frac{\psi}{2}) + 2\tan(90° - \phi) \right] \qquad (5)$$

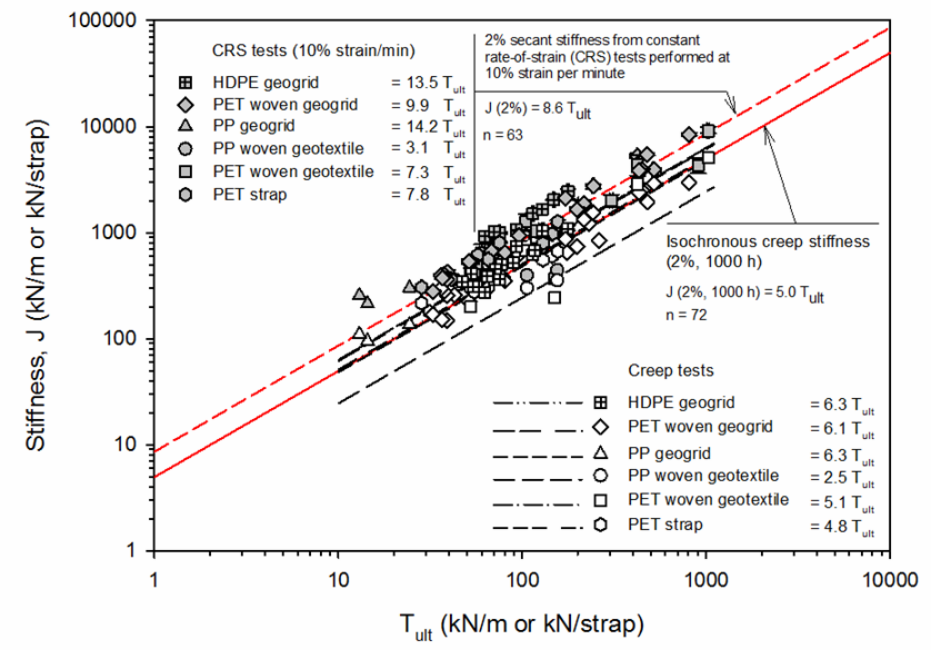

a)

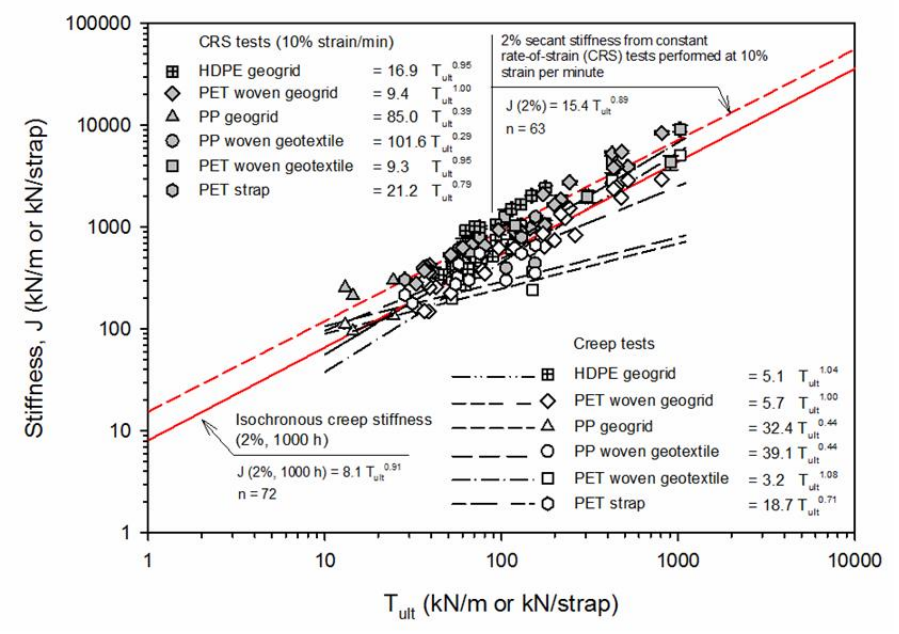

b)

Fig. 6. Stiffness versus T_{ult} at 2% strain from CRS tests and creep tests at 2% strain and 1000 h: a) linear relationship, and b) power function relationship [3].

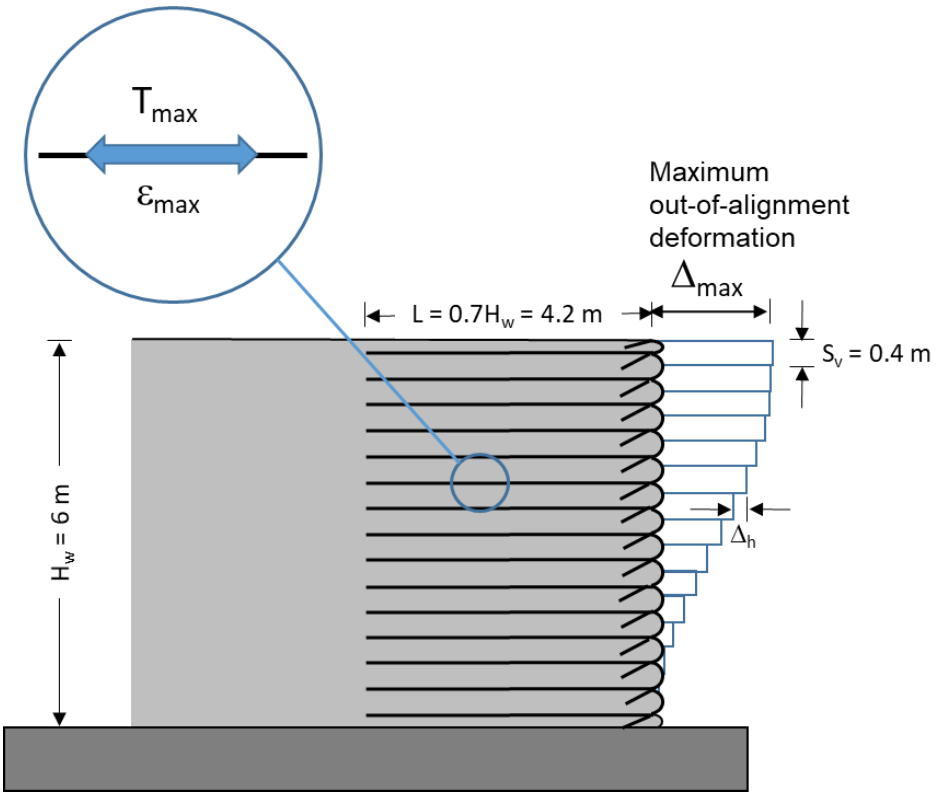

Fig. 7. Schematic of 6 m-high MSE wall with wrapped-face and 15 reinforcement layers [9].

Here, Δ_h is the incremental wall displacement taken with respect to the time the layer is placed in the wall during construction (i.e., moving datum displacement). Other parameters are K_a = active earth pressure coefficient, S_r = reinforcement layer coverage ratio, γ = soil unit weight, ϕ = friction angle from direct shear tests, Ψ = dilatancy angle ~ $\phi - 30° \geq 0$. For continuous sheet reinforcement $S_r = 1$, and for sheets of reinforcement placed with a gap or space between rolls, S_r is the fraction of the reinforcement layer that is continuous per unit length in the running wall direction. Summing Δ_h values up to each layer in turn is used to generate the wall profile at end of construction. Summing all values gives the maximum wall deflection at the top of the wall. Results of calculations reported by [9] using the typical range of reinforcement stiffness J in Figure 5, are shown in Figure 8. Note that $J = J_o(t)$ when $1/\chi(t) = 0$, and J decreases for the same value of $J_o(t)$ as $1/\chi(t)$ increases [Equation 3].

The shaded region in the figure is the range of maximum wall out-of-alignment reported by Bathurst et al. [11] based on specified and expected values found in the literature. A value of J = 1000 kN/m is judged to be a typical stiffness for sheet geosynthetic MSE walls. The plots in this figure show that wall deformation profiles using this model are sensitive to the choice of stiffness value.

3.2 Wall reinforcement loads

The Stiffness Method is now specified by AASHTO [12] in the US to compute maximum tensile loads in reinforcement layers for MSE walls under operational conditions. A signature feature of this method is the presence of the reinforcement stiffness in the formulation of the

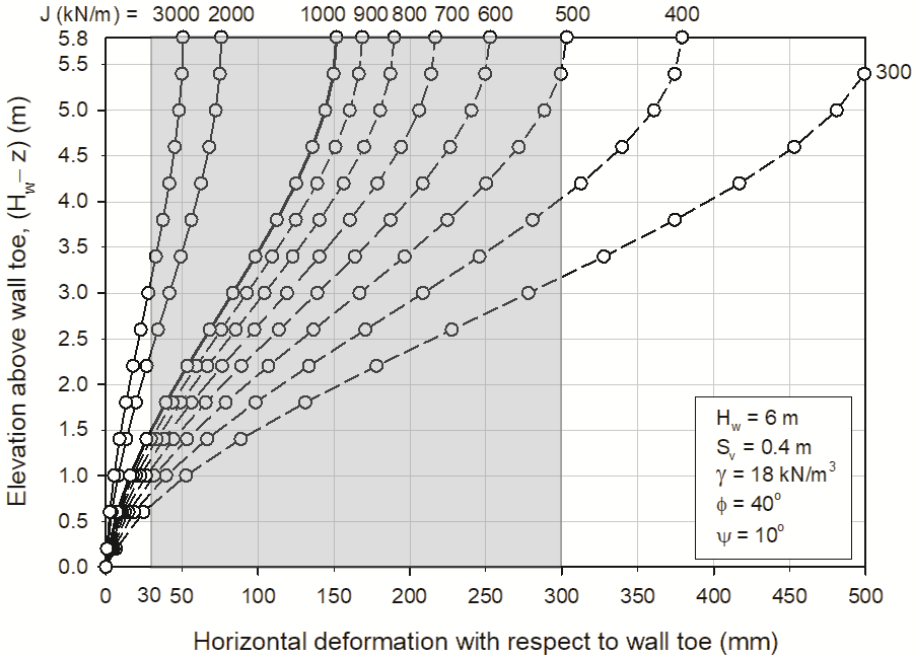

Fig. 8. Example wall out-of-alignment profiles [9] using the method of Jewell and Milligan [10].

maximum reinforcement load in each layer. For the same flexible face wall described in the previous section (Figure 7), the magnitude of maximum tensile load T_{max} in each reinforcement layer is computed as:

$$T_{max} = (S_v)^{1-\xi} H_w \times D_{tmax} \left[\gamma \tan^2\left(45° - \frac{\phi}{2}\right) (J \times S_r)^{\xi} \right] \frac{\alpha}{(p_a)^{\xi}} \qquad (6)$$

Here, the dimensionless coefficients are $\alpha = 0.16$, $\xi = 0.26$ and p_a = atmospheric pressure = 101 kPa. The non-dimensional coefficient D_{tmax} is a T_{max} distribution factor. All other parameters have been defined earlier. The calculation details can be found in [12, 13, 14]. The maximum value of $D_{tmax} = 1$. For design, the stiffness value J is taken as the isochronous secant stiffness value at $\varepsilon = 2\%$ and 1000 hours. Allen and Bathurst [15] showed that setting $D_{tmax} = 1$ gives the maximum reinforcement load in the wall (T_{mxmx}) computed as:

$$T_{mxmx} = (S_v)^{1-\xi} H_w \left[\gamma \tan^2\left(45° - \frac{\phi}{2}\right) (J \times S_r)^{\xi} \right] \frac{\alpha}{(p_a)^{\xi}} \qquad (7)$$

The corresponding maximum reinforcement strain from all layer ε_{mxmx} values is:

$$\varepsilon_{mxmx} = \frac{T_{mxmx}}{J \times S_r} = (S_v)^{1-\xi} H_w \left[\gamma \tan^2\left(45° - \frac{\phi}{2}\right) (J \times S_r)^{\xi-1} \right] \frac{\alpha}{(p_a)^{\xi}} \qquad (8)$$

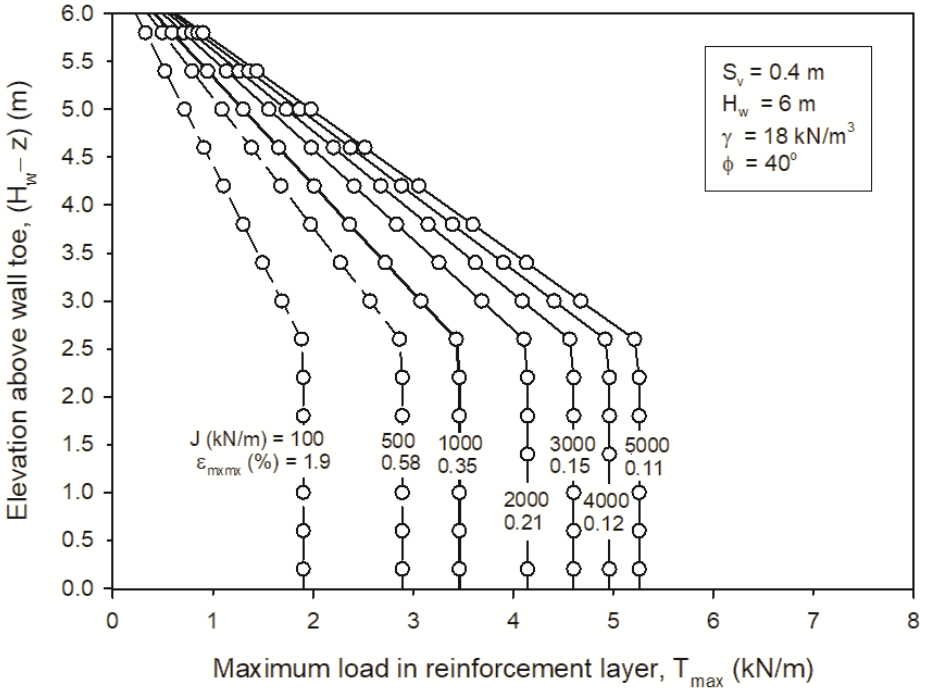

Fig. 9. Distribution of T_{max} and maximum reinforcement strain ε_{mxmx} at end of construction for 6 m-high wall constructed with 15 reinforcement layers [9].

The maximum tensile loads T_{max} and maximum strain ε_{mxmx} from all layers are plotted in Figure 9. The plots show that as the reinforcement becomes stiffer, the load in each layer increases and the maximum strain from all reinforcement layer becomes less.

The tangent isochronous load-strain hyperbolic model for the reinforcement (Equation 4) has been used in numerical finite difference models of MSE walls [e.g., 3]. The same qualitative trend of increasing maximum tensile load and decreasing maximum strain with increasing reinforcement stiffness has been observed in the results of these numerical models.

3.3 Reinforced granular fill over a void

The general analytical solution by Giroud et al. [16] can be used to compute the maximum strain and tensile load in a reinforcement layer spanning a long void at the base of a surcharged fill. The reinforced fill height is H and the void has an infinite length and width b (Figure 10). The fill peak friction angle $\phi > 20°$ and the ratio of maximum vertical deflection of the reinforcement (d) to width (b) is $d/b \leq 0.5$. For these conditions, the deflected geosynthetic profile follows the arc of a circle from which the maximum strain in the reinforcement is calculated as:

$$\varepsilon_{max} = 2\Omega \sin^{-1}\left(\frac{1}{2\Omega}\right) - 1 \quad \text{for } d/b < 0.5 \tag{9}$$

where,

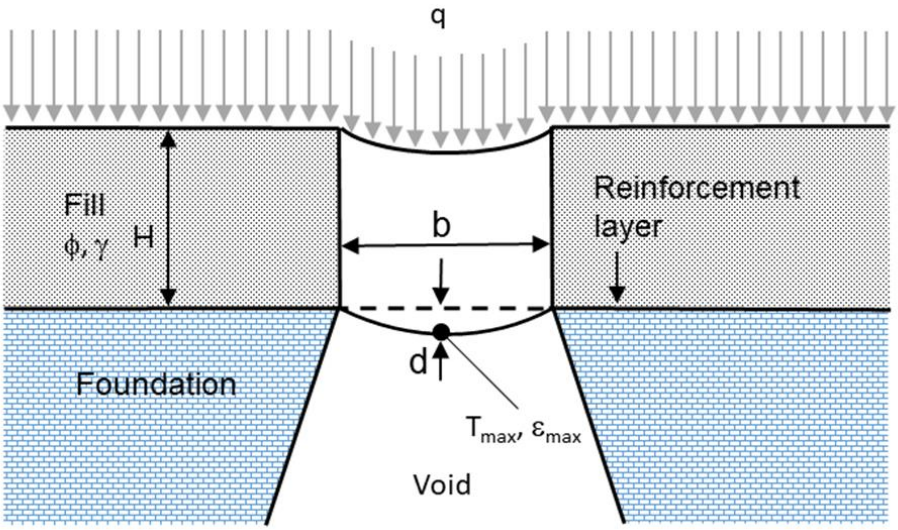

Fig. 10. Schematic for reinforced fill over a long void.

$$\Omega = 0.25\left(\frac{2d}{b} + \frac{d}{2b}\right) \tag{10}$$

The maximum tensile load in the reinforcement is computed as:

$$T_{max} = \left[2\gamma b\left[1 - e^{-0.5\,H/b}\right] + qe^{-0.5\,H/b}\right] b\Omega \tag{11}$$

The maximum mobilized tensile stiffness in the reinforcement can now be calculated as:

$$J_{mob} = T_{max} / \varepsilon_{max} \tag{12}$$

Equation 12 leads to the following design limit state where the mobilized geosynthetic stiffness must not exceed the available reinforcement stiffness ($J_{avail} > J_{mob}$).

Figure 11 shows the relationship between normalized deflection (d/b), maximum tensile strain (ε_{max}) and mobilized geosynthetic stiffness (J_{mob}). To use this figure, the normalized deflection, or a prescribed maximum strain, is entered and the minimum required geosynthetic stiffness is determined from the right-hand vertical axis. The figure shows that as the normalized deflection becomes less, the required stiffness increases. This can be understood to be the result of the circular arc geometry that is assumed as the starting point for the analysis method. Similar analyses were carried out by Naftchali and Bathurst [17] using three other analytical model approaches. However, qualitative features were similar to those shown in Figure 11 for all methods.

3.4 Reinforced granular fill over soft clay

Figure 12 shows a 2D numerical finite difference model for the problem of a strip footing seated on a thin reinforced granular layer overlying a soft to very soft undrained clay

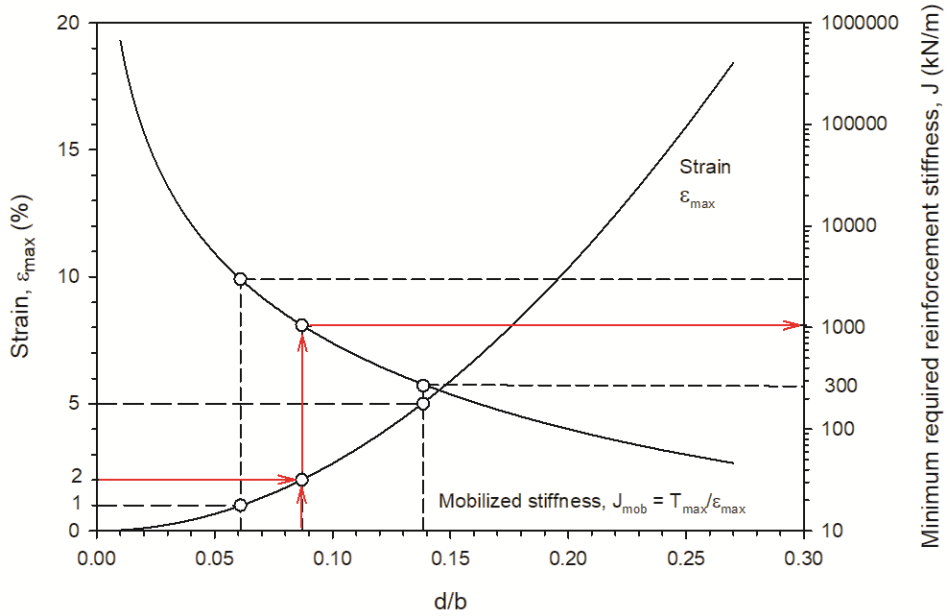

Fig. 11. Design chart to select minimum required geosynthetic stiffness to satisfy geosynthetic design stiffness limit state for a reinforced fill over a long void using the method of Giroud et al. [16] (after [3]).

foundation [8]. The simulations were carried out using the program 2D FLAC [18]. The purpose of the granular layer is to serve as a construction aide and to disperse the footing loads over a wider area of the weak foundation. For comparison purposes, simulations were also carried out with no granular layer (i.e., footing seated directly on the clay foundation) and with unreinforced granular layers. Analytical and numerical studies for the case of the footing seated directly on a clay foundation are common in the research literature. In practice, however, this is an unlikely occurrence; a granular layer is placed first for the reasons mentioned.

In this example, a rough rigid strip footing of width B = 1 m is placed on a granular layer of thickness D = 0.5 m overlying a weak undrained clay deposit with depth H = 5 m. A geogrid reinforcement layer is located 0.05 m above the bottom of the granular layer so that the open grid apertures of the geogrid can fully engage the granular soil. The reinforcement length is L = 5B = 5 m which was shown to be satisfactory to prevent pullout of the reinforcement during loading.

The soil zones were modelled as linear elastic-perfectly plastic materials and the geogrid sheet reinforcement for the plane-strain footing problem was simulated by FLAC CABLE elements. The tangent stiffness formulation for the two-component hyperbolic model was used as the constitutive model for the geogrid (Equation 4). The ultimate tensile strength of the reinforcement was taken as T_{ult} = J(ε = 2%, 1000 h)/5 (Figure 6a) [3]. However, tensile rupture of the reinforcement was not a concern in these simulations since the maximum tensile loads were well below T_{ult} in all cases.

A fully-bonded interface between the geogrid and granular soil was assumed to simulate the granular particles striking through the apertures of the geogrid. The granular layer was treated as a cohesionless linear-elastic plastic material with unit weight γ = 20 kN/m^3, Young's modulus E = 50 MPa, friction angle ϕ = 45° and dilation angle ψ = 10°. The foundation soil was assumed as a linear elastic-plastic material with undrained shear strength

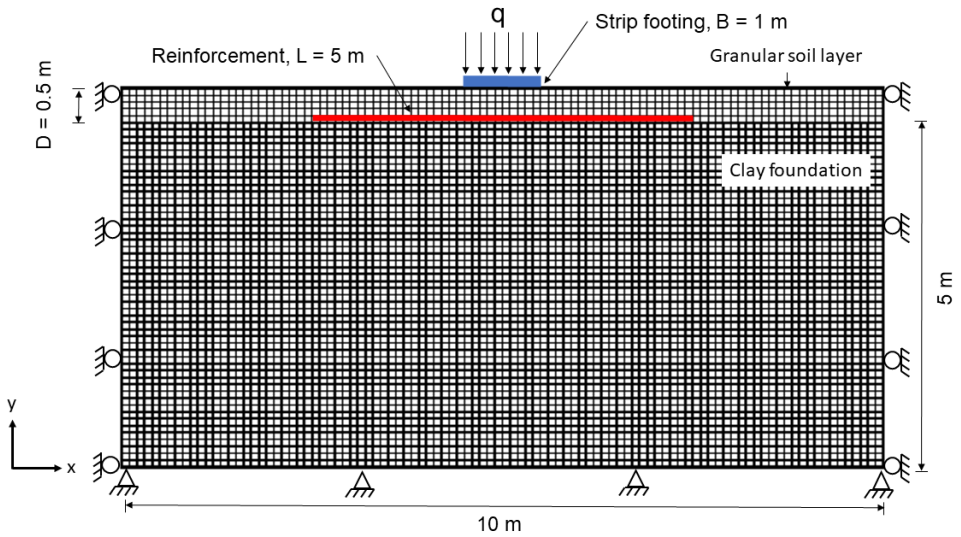

Fig. 12. Numerical FLAC grid showing problem geometry and component materials [8].

s_u = 5 to 25 kPa (i.e., soft to very soft clay). The undrained elastic modulus was taken as $E_u = 500 \times s_u$.

In each simulation, the footing was advanced in increments of 0.001 m. A total of 100 steps was found to be sufficient to develop a footing resistance consistent with the notion of ultimate bearing capacity. The program was executed using the large strain option in FLAC.

3.4.1 Results

Figure 13 shows a comparison of bearing pressure versus footing settlement for the three footing cases in this study. In each case the undrained shear strength of the clay foundation is s_u = 5 kPa. Solutions for the reinforced granular case are plotted for different constant isochronous stiffness values (i.e., $J_o(t)$ = constant, $1/\chi(t) = 0$). The plots show that there is a significant increase in bearing capacity for the same settlement by placing the footing on a granular layer compared to placing the footing directly on the clay foundation. The figure also shows that the benefit of including the reinforcement at the base of the granular layer is only detectable once sufficient deformation occurs, which in this example is well beyond a serviceability deformation of 25 mm. While the bearing pressure increases with increasing geogrid stiffness, the practical increase in ultimate bearing capacity compared to the unreinforced granular layer case is modest (e.g., maximum of 20% at a settlement of 0.1 m and $J_o(t)$ = 3000 kN/m).

Figure 14 shows the development of tensile load in the reinforcement layer as the footing is displaced downward. For the same settlement, the tensile load increases with increasing reinforcement stiffness.

Figure 15 shows the influence of the isochronous stiffness curvature parameter $\chi(t)$ on bearing pressure-settlement response for the case of a reinforcement layer with stiffness $J_o(t)$ = 1000 kN/m. The influence of $\chi(t)$ on bearing pressure is judged to be small in this example. However, the influence of $\chi(t)$ on maximum tensile load is larger as shown in Figure 16. The largest tensile loads are generated for the case of constant linear stiffness with strain (i.e., $1/\chi(t) = 0$).

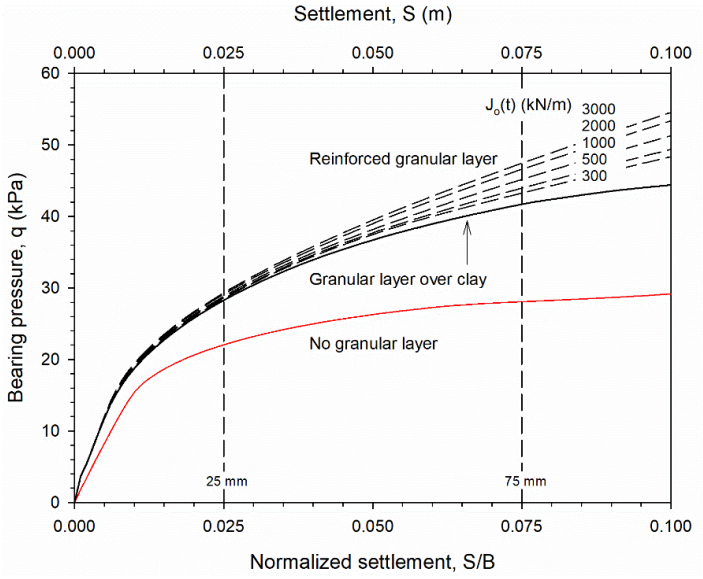

Fig. 13. Comparison of bearing pressure settlement response for reinforced and unreinforced granular layer and for the case of the footing seated directly on the clay foundation. (s_u = 5 kPa, $1/\chi(t) = 0$) [8].

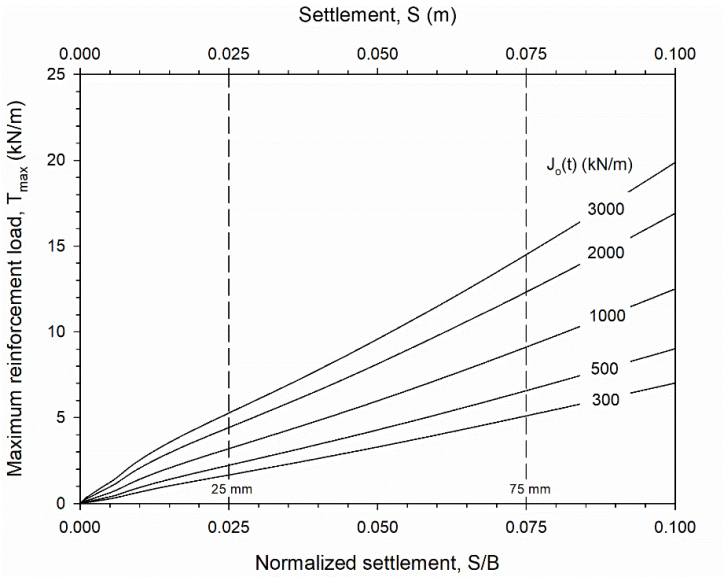

Fig. 14. Influence of reinforcement stiffness parameter $J_o(t)$ maximum reinforcement tensile load-settlement response. (s_u = 5 kPa, $1/\chi(t) = 0$) [8].

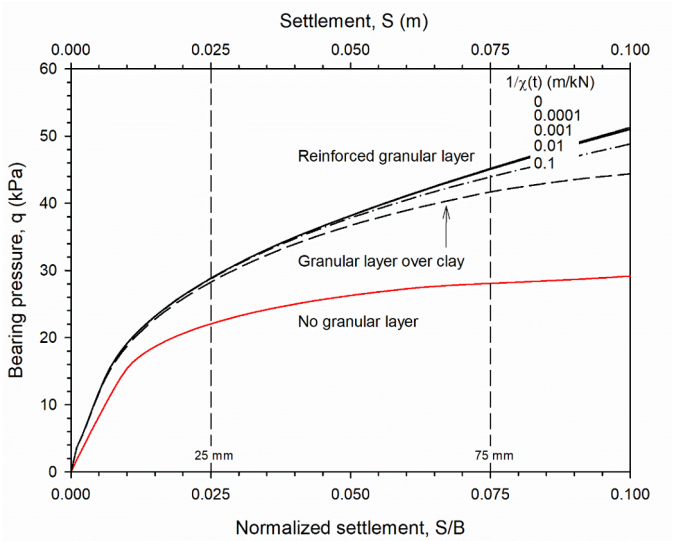

Fig. 15. Comparison of bearing pressure settlement response for reinforced and unreinforced granular layer and for the case of the footing seated directly on the clay foundation (s_u = 5 kPa, $J_o(t)$ = 1000 kN/m) [8].

The plots in Figure 17 show that the distributions of tensile load at ultimate bearing capacity are saddle-shaped with the peak values located below the footing edges. As the undrained shear strength of the clay foundation becomes less for the same values of $J_o(t)$ = 1000 kN/m and $\chi(t)$, the magnitudes of tensile load decrease. The plots also show that for the same value of $J_o(t)$, the loads and the length over which load is mobilized in the reinforcement are less as the curvature parameter for the hyperbolic model is reduced.

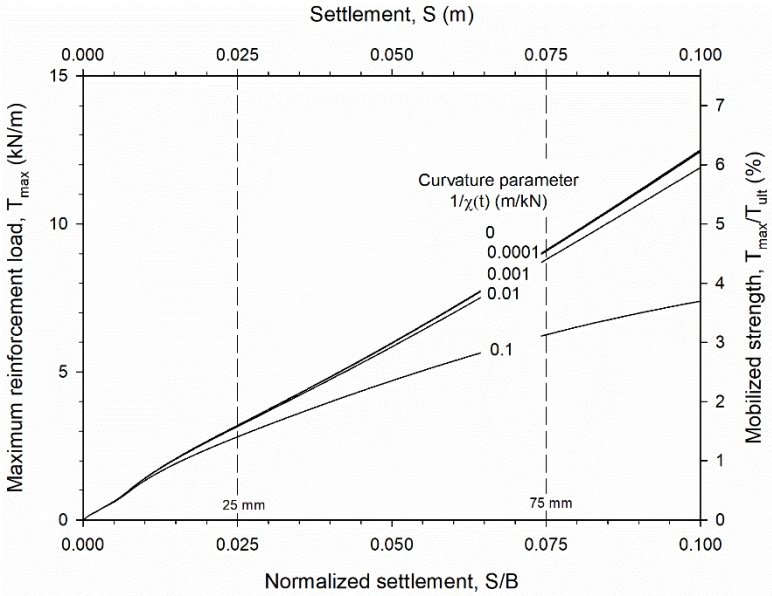

Fig. 16. Influence of reinforcement isochronous stiffness curvature parameter $\chi(t)$ on maximum reinforcement tensile load-settlement response. (s_u = 5 kPa, $J_o(t)$ = 1000 kN/m, T_{ult} = 200 kN/m) [8].

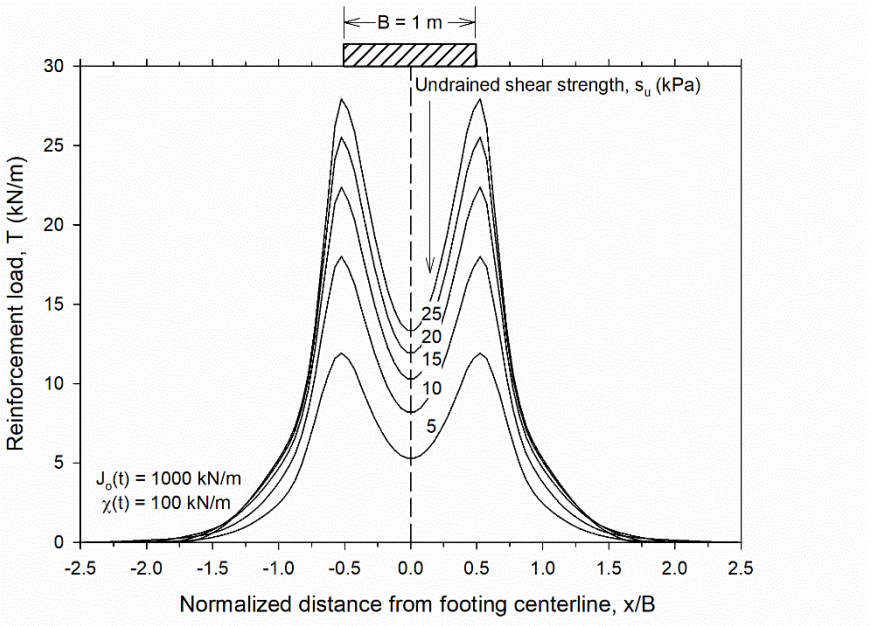

a)

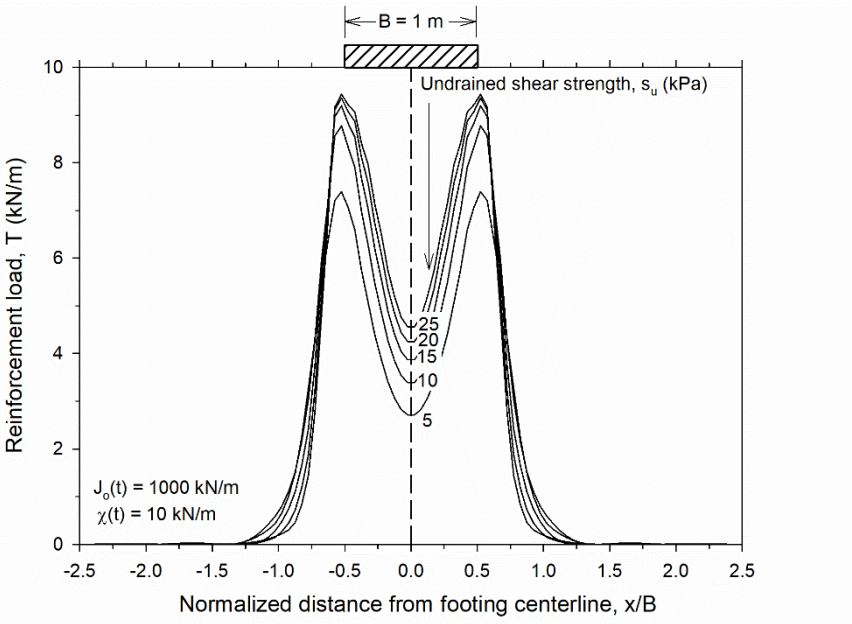

b)

Fig. 17. Distribution of load T in geosynthetic reinforcement at ultimate footing bearing capacity at S/B = 0.1 (B = 1 m, $J_o(t)$ = 1000 kN/m): a) $\chi(t)$ = 100 kN/m, and; b) $\chi(t)$ = 10 kN/m [8].

The numerical model described here was used to calibrate an analytical model for the ultimate bearing capacity of the same 0.5 m-thick reinforced granular layer over a soft undrained clay foundation [8]. Their formulation contains a non-dimensional reinforcement bearing capacity factor that is a function of $J_o(t)$ and curvature parameter $\chi(t)$.

Finally, Jamshidi Chenari and Bathurst [19] used a similar finite difference model to carry out reliability analyses for the same three foundation scenarios. In these stochastic analyses they considered spatially variable soft clay foundation soil. To simplify analyses, the reinforcement stiffness was assumed as a linear-elastic plastic material with constant isochronous stiffness parameter $J_o(t)$ and the curvature parameter taken as $\chi(t) = 0$. The program was executed using the small strain option in FLAC to keep Monte Carlo simulation run-times manageable. An important outcome from this most recent work are design charts to estimate the deterministic design bearing capacity that is required to satisfy a range of target reliability index for the case of a strip footing seated on a reinforced granular layer overlying very soft to soft undrained clay.

4 Conclusions

This paper reviews recent published work by the writers that is focused on the load-strain-time behaviour (stiffness) of geosynthetic reinforcement materials under tensile load. A two-component hyperbolic model has been developed that can be used to model the secant and tangent isochronous stiffness behaviour of a wide range of geosynthetic product types used in soil reinforcement applications. Some of the main conclusions from this work are:

1. Using the secant stiffness deduced from conventional rapid in-air constant rate-of-strain (CRS) tests can overestimate the stiffness of these materials under constant load, sometimes by very large margins. The consequences of using CRS data are that MSE wall deformations will be under-estimated and tensile loads under operational conditions will be over-estimated.
2. The formulations for the secant isochronous load-strain behaviour are suitable for analytical models used to estimate MSE wall deformations and loads at end of construction for walls under operational conditions, and for the problem of a reinforced fill over a void. The same model expressed using the tangent secant stiffness can be used in numerical finite difference and finite element models.
3. Useful linear and non-linear approximations are available from [3] to link isochronous secant stiffness values for different strains and isochronous times to the ultimate tensile strength of the reinforcement for different product classifications using conventional CRS tests carried out at 10% strain/minute.

In this paper, only brief outlines of portions of the cited work have been attempted. The interested reader is directed to these publications for additional details.

References

1. A. McGown, Andrawes, K.Z, Yeo, K.C., Dubois, D., *The load-strain-time behaviour of Tensar geogrids*. In Proceedings of Polymer Grid Reinforcement, Thomas Telford Publishing (1984)
2. A. McGown, A., Paine, N., Dubois, D., Andrews, K.Z., Jewell, R.A., *Use of geogrid properties in limit equilibrium analysis*. In Proceedings of Polymer Grid Reinforcement. Thomas Telford Publishing (1984)
3. R.J. Bathurst, Naftchali, F.M. Geotex & Geom **49** (2021)
4. ASTM D5262-97. Standard Test Method for Evaluating the Unconfined Tension Creep Behavior of Geosynthetics. ASTM Int (1997)

5. ASTM D6992-03. Standard Test Method for Accelerated Tensile Creep and Creep-Rupture of Geosynthetic Materials Based on Time-Temperature Superposition Using the Stepped Isothermal Method. ASTM Int (2003)
6. ASTM D4595-17. Standard Test Method for Tensile Properties of Geotextiles by the Wide-Width Strip Method. ASTM Int (2017)
7. ASTM D6637/D6637M-15. Standard Test Method for Determining Tensile Properties of Geogrids by the Single or Multi-Rib Tensile Method. ASTM Int (2015)
8. R. Jamshidi Chenari, Bathurst, R.J. Geotex & Geom **51** (2023)
9. R.J. Bathurst, Naftchali, F.M. Geotex & Geom **51** (2023)
10. R.A. Jewell, Milligan, G.W.E. *Deformation calculation for reinforced soil walls*. In Proceedings of 12th International Conference on Soil Mechanics and Foundation Engineering (1989)
11. R.J. Bathurst, Miyata, Y., Allen, T.M. *Facing displacements in geosynthetic reinforced soil walls*. In Proceedings of Earth Retention Conference 3 (ER2010), ASCE Geo-Institute (2010)
12. AASHTO. *LRFD Bridge Design Specifications*. 9th Ed. American Association of State Highway and Transportation Officials (AASHTO) (2020)
13. T.M. Allen, Bathurst, R.J. ASCE J of Geotech & Geoenv Eng **141** (2015)
14. T.M. Allen, Bathurst, R.J. ASCE J of Geotech & Geoenv Eng **144** (2018)
15. T.M. Allen, Bathurst, R.J. Geosyn Int **26** (2019)
16. J.P. Giroud, Bonaparte, R., Beech, J.F., Gross, B.A. Geot & Geom **9** (1990)
17. F.M. Naftchali, Bathurst, R.J. Geosyn Int 30 (2023)
18. Itasca. FLAC 2D: Fast Lagrangian Analysis of Continua. Version 8.0 [computer program]. Itasca Consulting Group, Inc., Minneapolis, Minn. (2011)
19. R. Jamshidi Chenari, Bathurst, R.J. ASCE J of Geotech & Geoenv Eng (in press) (2023)